Journal of Guidance, Control, and Dynamics, Vol. 43, No. 9, 2020, pp. 1727–1732. doi: http://doi.org/10.2514/1.G005214

Trajectory Analysis of a Sun-Facing Solar Sail with Optical Degradation

Marco Bassetto*, Alessandro A. Quarta†, Giovanni Mengali‡,
and Vittorio Cipolla§
Department of Civil and Industrial Engineering, University of Pisa, I-56122 Pisa, Italy

Nomenclature

a	=	semimajor axis, au
$\boldsymbol{a}_p$	=	propulsive acceleration, m/s^2
c_1, c_2	=	constants of integration, see Eqs. (13)
$\boldsymbol{e}$	=	eccentricity vector, with $e \triangleq \|\boldsymbol{e}\|$
O	=	spacecraft center-of-mass
p	=	semilatus rectum, au
r	=	Sun-spacecraft distance, au
$\hat{\boldsymbol{r}}$	=	radial unit vector
r_a	=	aphelion radius, au
r_p	=	perihelion radius, au
t	=	time, days
T	=	sail film degradation half-life, years
$\mathcal{T}_O$	=	polar reference frame
u	=	radial component of spacecraft velocity, km/s
v	=	transverse component of spacecraft velocity, km/s
β	=	sail lightness number
ϵ	=	sail film degradation parameter, 1/s
η	=	sail film reflectivity
θ	=	azimuthal angle, rad
$\hat{\boldsymbol{\theta}}$	=	transverse unit vector
λ	=	dimensionless parameter, see Eq. (10)
$\mu_\odot$	=	Sun's gravitational parameter, km^3/s^2
ν	=	true anomaly, rad
ξ	=	dimensionless threshold value
ρ	=	dimensionless variable
ω	=	osculating orbit orientation, rad

Subscripts

0	=	initial
$\oplus$	=	at 1 au from the Sun
max	=	maximum
min	=	minimum

Superscripts

$\dot{}$	=	time derivative
$'$	=	derivative with respect to θ
$\tilde{}$	=	steady-state value

Introduction

Solar sails generate thrust by means of thin metalized polymer films, which extract momentum from the impinging photons coming from the Sun [1–6] . The dynamics of a solar sail-based spacecraft is usually studied under the simplifying assumption that the optical properties of its reflective membrane are time-invariant. Such an assumption is useful in a preliminary mission design phase, because it allows the problem to be considerably simplified from a mathematical point of view. In practice, the problem is more involved since a long-term exposure to radiations and to solar wind particles causes a degradation of the metalized polymer film. Such an unavoidable phenomenon reduces the solar sail performance by inducing a decrease of both its lightness number and the maximum reachable angle between the Sun-sail line and the thrust vector. A more refined study of the solar sail trajectory should therefore consider the polymer film aging, especially in the case of long-duration missions.

Extensive test campaigns have not yet been made to deeply investigate the complex phenomenon of sail film degradation, which is therefore difficult to model with accuracy. In this regard, Vulpetti and Scaglione [7] have processed some experimental data related to aluminium in order to average its thermo-optical properties over the spectrum of the incident solar photons. They [8] have also investigated the possibility of exploiting the degradation of plastic materials due to ultraviolet (UV) radiation or atomic oxygen in order to obtain an entirely metallic solar sail (which is useful, for example, for performing an angular momentum reversal maneuver). Khassanchine et al. [9] have described the effects of electron radiation on outgassing of spacecraft materials, Prosvirikov et al. [10] have reported the measurements of hemispherical reflectance for some thermal

*Research Assistant, marco.bassetto@ing.unipi.it
†Professor, a.quarta@ing.unipi.it. Associate Fellow AIAA. (**corresponding author**)
‡Professor, g.mengali@ing.unipi.it. Senior Member AIAA.
§Assistant Professor, vittorio.cipolla@unipi.it. Member AIAA.

control coatings within the spectral range $0.2 - 2.5\,\mu$m, whereas Edwards et al. [11] have quantified the effect of the space environment on thermo-optical and mechanical properties of candidate sail materials, such as aluminum coated Mylar, Teonex, and Colorless Polyimide. More recently, Kezerashvili and Matloff [12] have investigated the interaction between solar radiation and sail materials, showing that the latter are partially ionized by solar UV and low-energy electrons. Using a theoretical approach, Kezerashvili [13] has analyzed the degradation of solar sail materials due to their interaction with electromagnetic waves and induced by the radiation from low- and high-energy electrons, protons, and α-particles emitted by the Sun. In particular, it has been shown [13] that the space environment causes a reduction of the reflectivity coefficient, which in turn increases the solar sail equilibrium temperature. Moreover, Sznajder et al. [14–16] have proposed and empirically proved the formation of tiny molecular hydrogen bubbles on metallic surfaces by simulating the space environment in terms of temperature, proton dose, and kinetic energy of the incident particles, while Ancona and Kezerashvili [17] have shown that the degradation of sail materials is also due to the dependence of emissivity on temperature. Finally, Pino et al. [18] have analyzed the influence of wrinkles and creases (which can actually be seen as degrading effects) on the solar sail performance.

In the early 2000s, Rios-Reyes and Scheeres [19] have defined an analytical model for the description of the thrust and torque generated by a solar sail of arbitrary shape and optical properties, while Dachwald et al. [20, 21] have proposed a parametric model to describe the degradation of an optical solar sail, in which the time variation of the optical coefficients is provided as a function of the absorbed radiation dose. Using the latter model, Ref. [22] has derived the optimal control law with an indirect optimization method, and investigated the effects of different degradation behaviors in an Earth-Mars transfer. The performance of a degrading solar sail has been analyzed in Ref. [23] in other heliocentric mission cases, such as a Mercury rendezvous, fast missions to Neptune and to the heliopause, and the generation of artificial Lagrangian points. Later, McInnes [24] has presented an approximate closed-form solution for solar sail spiral trajectories with film degradation, starting from the parametric model conceived by Dachwald et al. [20, 21]. In particular, Ref. [24] provides the time evolution of the solar sail orbital radius in an implicit form, assuming a quasi-circular spiral with a constant sail pitch angle, that is, a fixed attitude with respect to the current Sun-sail line.

The aim of this Note is to extend the work by McInnes [24], by specializing those results to the case of a Sun-facing solar sail, that is, a solar sail with a reflective membrane that is always perpendicular to the Sun-spacecraft line. The advantage of a sail attitude remaining constant relative to the Sun-sail line is that it can be passively maintained through a suitable choice of the sail shape [25]. In this configuration, a solar sail generates a purely outward radial propulsive acceleration, which makes a number of heliocentric scenarios possible, such as the maintenance of heliostationary conditions [26], the formation of artificial collinear Lagrangian points [27–29], or a heliocentric in-orbit repositioning [30]. In particular, this Note gives the closed-form solution of the heliocentric motion of a Sun-facing solar sail with optical degradation. The orbital radius, the semimajor axis, the eccentricity, and the in-plane osculating orbit orientation are all explicitly given as a function of the spacecraft angular position. The availability of an analytical form for the solar sail trajectory represents a very useful tool for mission analysis purposes, as it considerably reduces the computational cost that would otherwise be required for the simulation of a large number of possible trajectories.

The Note is organized as follows. The next section extends the results of Ref. [24] to the special case of a Sun-facing solar sail, and derives the analytical polar form of the spacecraft trajectory. The steady-state solution is then analyzed and discussed, with an emphasis on the special case of circular parking orbits. After the discussion of an exemplary mission case, the Note ends with some concluding remarks.

Trajectory analysis

Consider a solar sail-based spacecraft that initially covers a heliocentric (Keplerian) parking orbit of semilatus rectum p_0 and eccentricity $e_0 < 1$. The sail deployment occurs at the initial time $t = t_0 \triangleq 0$, and the assumption is made that the sail attitude remains Sun-facing at any time, that is, the reflective membrane is always perpendicular to the Sun-spacecraft line.

Due to the radiation dose, the optical and mechanical properties of the reflective film begin to degrade after the deployment, so to progressively reduce the propulsive performance of the solar sail. Assume that the sail film degradation is mathematically described by the parametric model proposed by Dachwald et al. [20, 22, 23]. In a Sun-facing sail, the propulsive acceleration vector $\boldsymbol{a}_p$ is purely radial and may be written by adapting the thrust model discussed in Ref. [24], that is

$$\boldsymbol{a}_p = \frac{\beta\,(\eta+1)\,\mu_\odot}{2\,r^2}\,\hat{\boldsymbol{r}} \tag{1}$$

where $\mu_\odot$ is the Sun's gravitational parameter, r is the Sun-sail distance, $\hat{\boldsymbol{r}}$ is the Sun-spacecraft unit vector, $\beta > 0$ is the sail lightness number [31], and $\eta \in [0,\,1]$ is the time-varying reflectivity coefficient [24]. The condition $\eta = 1$ (or $\eta = 0$) corresponds to the case in which the incident photons are all specularly reflected (or absorbed) by the sail, which therefore behaves like an ideal mirror (or a black body). According to Refs. [22, 23], the time variation of η for a Sun-facing sail can be written as

$$\dot{\eta} = -\epsilon\,\eta\,\left(\frac{r_\oplus}{r}\right)^2 \qquad \text{with} \qquad \eta(t_0) \triangleq \eta_0 = 1 \tag{2}$$

where $r_\oplus \triangleq 1\,\text{au}$ is a reference distance, while

$$\epsilon = \frac{\ln(2)}{T} \tag{3}$$

is a sort of "degradation parameter", which depends on the sail degradation half-life $T > 0$, the latter being defined as the time interval required for the parameter η to halve its initial value η_0 [22, 23].

Introduce now a polar reference frame $\mathcal{T}(O;\,r,\,\theta)$, with unit vectors $\hat{\boldsymbol{r}}$ and $\hat{\boldsymbol{\theta}}$, of which the origin O coincides with the Sun's center-of-mass, while θ is the azimuthal angle measured counterclockwise from the initial Sun-sail direction; see Fig. 1. Because the propulsive acceleration vector is radial, the semilatus rectum p is a constant of motion (i.e., $p \equiv p(t_0) \triangleq p_0$), and the spacecraft dynamics is described by the following system of nonlinear differential equations

$$\dot{r} = u \quad , \quad \dot{\theta} = \frac{\sqrt{\mu_\odot\,p_0}}{r^2} \quad , \quad \dot{u} = -\frac{\mu_\odot}{r^2} + \frac{\mu_\odot\,p_0}{r^3} + a_p \tag{4}$$

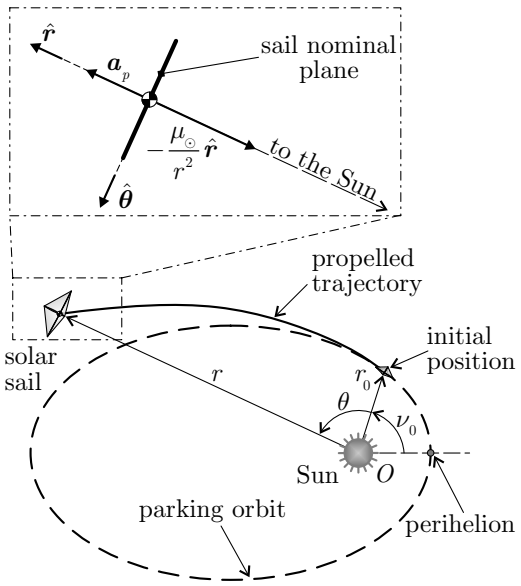

Figure 1 Reference frame and sail propulsive acceleration vector.

where u is the radial velocity, while $a_p \triangleq \|\boldsymbol{a}_p\|$ is the magnitude of the propulsive acceleration vector of Eq. (1). Note also that the term $\mu_\odot\, p_0/r^3$ represents the centrifugal acceleration in the case of purely radial thrust (in fact, $\sqrt{\mu_\odot\, p_0}$ is the constant specific angular momentum of the spacecraft orbit). The initial conditions are

$$r(t_0) \triangleq r_0 = \frac{p_0}{1 + e_0\, \cos\nu_0} \quad , \quad \theta(t_0) = 0 \quad , \quad u(t_0) \triangleq u_0 = \sqrt{\frac{\mu_\odot}{p_0}}\, e_0\, \sin\nu_0 \tag{5}$$

where $\nu_0 \in [0,\, 2\pi)$ rad is the initial true anomaly; see Fig. 1.

The system of Eqs. (2) and (4) may be conveniently rewritten by using θ as the independent variable. To that end, consider the Bürdet-Ferrandiz regularization scheme [32–35], and introduce the dimensionless variable

$$\rho \triangleq \frac{p_0}{r} - 1 \tag{6}$$

Note that $\rho \equiv e\, \cos\nu$, where e and ν are the eccentricity and true anomaly of the sail osculating orbit, respectively. In other words, the dimensionless variable ρ represents the projection of the osculating orbit eccentricity vector $\boldsymbol{e}$ along the radial unit vector $\hat{\boldsymbol{r}}$. With the aid of Eq. (6), Eqs. (2) and (4)-(5) become

$$\rho'' + \rho + \frac{\beta\, (1+\eta)}{2} = 0 \tag{7}$$

$$\eta' + \lambda\, \eta = 0 \tag{8}$$

$$\rho(\theta_0) = e_0\, \cos\nu_0 \quad , \quad \rho'(\theta_0) = -e_0\, \sin\nu_0 \quad , \quad \eta(\theta_0) = 1 \tag{9}$$

where the prime symbol denotes a derivative taken with respect to θ, while

$$\lambda \triangleq \frac{\epsilon\, r_\oplus^2}{\sqrt{\mu_\odot\, p_0}} \equiv \frac{\ln(2)\, r_\oplus^2}{T \sqrt{\mu_\odot\, p_0}} \tag{10}$$

is a dimensionless positive constant, which is typically less than 1. For example, assuming a sail half-life of one year [24] and a semilatus rectum of the parking orbit of one astronomical unit, Eq. (10) gives a value of λ of about one tenth.

Equations (7)-(9) can be solved using standard methods to obtain the variation of $\{\rho,\, \eta\}$ with respect to θ, and the result is

$$\rho = c_1\, \cos\theta + c_2\, \sin\theta - \frac{\beta}{2}\, \left(1 + \frac{e^{-\lambda\, \theta}}{1+\lambda^2}\right) \tag{11}$$

$$\eta = e^{-\lambda\, \theta} \tag{12}$$

where $\{c_1,\, c_2\}$ are two constants of integration, given by

$$c_1 = e_0\, \cos\nu_0 + \frac{\beta\, \left(2+\lambda^2\right)}{2\, (1+\lambda^2)} \quad , \quad c_2 = -\frac{\beta\, \lambda}{2\, (1+\lambda^2)} - e_0\, \sin\nu_0 \tag{13}$$

The polar form of the solar sail trajectory, that is, the function $r = r(\theta)$, can be derived from Eqs. (6) and (11) as

$$r = \frac{p_0}{1 + c_1\, \cos\theta + c_2\, \sin\theta - \frac{\beta}{2}\, \left(1 + \frac{e^{-\lambda\, \theta}}{1+\lambda^2}\right)} \tag{14}$$

while the radial (u) and azimuthal (v) components of the spacecraft velocity are given by

$$u = -\sqrt{\frac{\mu_\odot}{p_0}}\rho' \quad , \quad v = \frac{\sqrt{\mu_\odot\, p_0}}{r} \equiv \sqrt{\frac{\mu_\odot}{p_0}}\,(1+\rho) \tag{15}$$

where

$$\rho' = c_2\,\cos\theta - c_1\,\sin\theta + \frac{\beta\,\lambda\,e^{-\lambda\,\theta}}{2\,(1+\lambda^2)} \tag{16}$$

The closed form expression (14) of the propelled trajectory extends the results by McInnes [24], which provides an implicit solution when the sail pitch angle is constant, to the special case of a Sun-facing sail.

Using Eq. (15) for the velocity components, it may be verified that $\boldsymbol{e}\cdot\hat{\boldsymbol{\theta}} = \rho'$, from which

$$\boldsymbol{e} = \rho\,\hat{\boldsymbol{r}} + \rho'\,\hat{\boldsymbol{\theta}} \tag{17}$$

The semimajor axis and the eccentricity of the osculating orbit may therefore be written as

$$a = \frac{p_0}{1-\rho^2-(\rho')^2} \quad , \quad e = \sqrt{\rho^2+(\rho')^2} \tag{18}$$

The orientation of the osculating orbit depends on the angle ω between the direction of vector $\boldsymbol{e}$ and the initial Sun-sail line; see Fig. 2. From the figure, the angle ω is given by

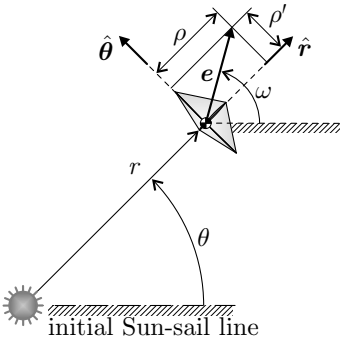

Figure 2 Eccentricity vector components and angle ω.

$$\omega = \theta + \arctan\left(\frac{\rho'}{\rho}\right) \equiv \theta + \arctan\left[\frac{c_2\,\cos\theta - c_1\,\sin\theta + \dfrac{\beta\,\lambda\,e^{-\lambda\,\theta}}{2\,(1+\lambda^2)}}{c_1\,\cos\theta + c_2\,\sin\theta - \dfrac{\beta}{2}\left(1+\dfrac{e^{-\lambda\,\theta}}{1+\lambda^2}\right)}\right] \tag{19}$$

Finally, the sail true anomaly ν along the osculating orbit is simply $\nu = \theta - \omega$.

For exemplary purposes, the variation of $\{a,\, e,\, \omega,\, \eta\}$ with θ is shown in Fig. 3 when $p_0 = 1\,\text{au}$, $e_0 = 0$, $\beta = (1\,\text{mm/s}^2)/(\mu_\odot/r_\oplus^2) \simeq 0.1686$, and $T = 1\,\text{year}$. Note that this case is consistent with the deployment of a medium-high performance solar sail on a parabolic escape trajectory from the Earth, with the simplifying assumption that the planet's orbit is circular.

Steady-state solution

When the flight time (or the azimuthal angle) approaches infinity, the sail reflectivity $\eta \to 0$. In other terms, after a sufficiently long interval, which depends on the sail degradation half-life T, η is smaller than a positive threshold value $\xi \ll 1$, and may be neglected. Recalling Eq. (12), when

$$\theta \geq \widetilde{\theta} \triangleq -\frac{\ln\xi}{\lambda} \tag{20}$$

the solar sail trajectory (14) reduces to

$$r \simeq \widetilde{r} \triangleq \frac{p_0}{1 + c_1\,\cos\theta + c_2\,\sin\theta - \beta/2} \tag{21}$$

while Eqs. (18) yield the steady-state osculating orbit semimajor axis and eccentricity as

$$a \simeq \widetilde{a} \triangleq \frac{p_0}{1-\widetilde{e}^2} \quad , \quad e \simeq \widetilde{e} \triangleq \sqrt{\beta^2/4 - \beta\,(c_1\,\cos\theta + c_2\,\sin\theta) + c_1^2 + c_2^2} \tag{22}$$

where $\{c_1,\, c_2\}$ are given by Eqs. (13). Note that Eq. (21) can also be obtained by observing that, when $\eta = 0$, the solar sail covers a non-Keplerian elliptic orbit where the equivalent Sun's gravitational parameter is $\mu_\odot\,(1-\beta/2)$.

When the degradation process has finished, it is also possible to find an analytical expression of the extremes of the osculating orbit eccentricity $\widetilde{e}$ (or semimajor axis $\widetilde{a}$). In fact, enforcing the necessary condition $\partial\widetilde{e}/\partial\theta = 0$ into the second of Eqs. (22), the maximum and minimum values of $\widetilde{e}$ are given by

$$\widetilde{e}_{\max} \triangleq \max\{\widetilde{e}\} = \sqrt{c_1^2+c_2^2} + \frac{\beta}{2} \quad , \quad \widetilde{e}_{\min} \triangleq \min\{\widetilde{e}\} = \left|\sqrt{c_1^2+c_2^2} - \frac{\beta}{2}\right| \tag{23}$$

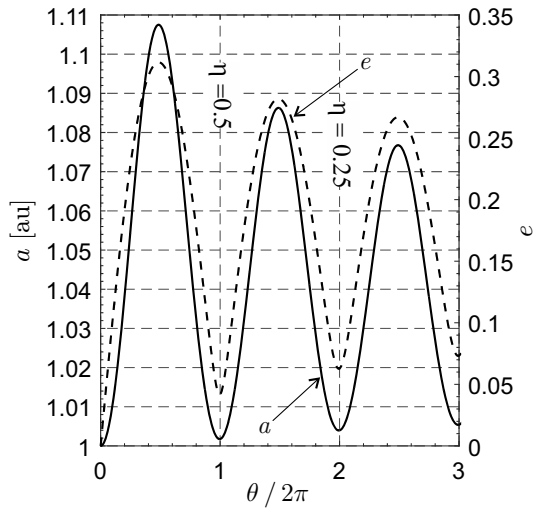

a) Variation of $\{a,\, e,\, \eta\}$ with θ.

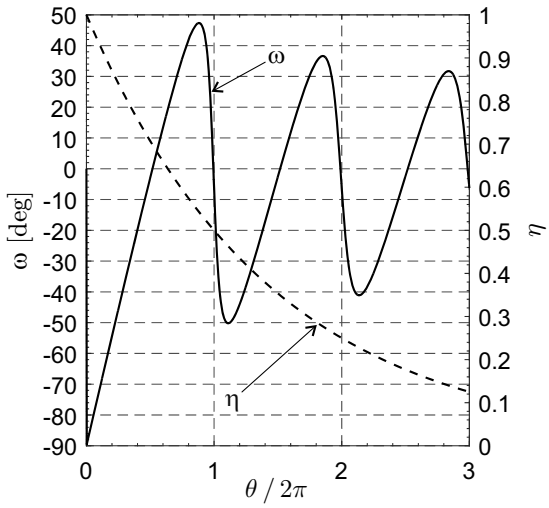

b) Variation of $\{\omega,\, \eta\}$ with θ.

Figure 3 Sail trajectory characteristics when $p_0 = 1\,\text{au}$, $e_0 = 0$, $\beta = (1\,\text{mm/s}^2)/(\mu_\odot/r_\oplus^2)$, and $T = 1\,\text{year}$.

which are reached when

$$\theta = \widetilde{\theta} \triangleq \arctan\left(\frac{c_2}{c_1}\right) + k\,\pi \quad \text{with} \quad k \in \mathbb{N} \cap k \geq k_{\min} \triangleq \left\lceil \frac{1}{\pi}\left[\widetilde{\theta} - \arctan\left(\frac{c_2}{c_1}\right)\right]\right\rceil \tag{24}$$

where $\lceil \square \rceil$ is the ceiling function. For example, assuming $\xi = 10^{-2}$ and considering the simplified case when $p_0 = 1\,\text{au}$, $e_0 = 0$, $\beta = 0.1686$, and $T = 1\,\text{year}$, Eq. (20) gives $\widetilde{\theta} \simeq 41.7446\,\text{rad}$, whereas Eq. (24) gives $k_{\min} = 14$. Figure 4 shows the variation of $\widetilde{e}_{\max}$ and $\widetilde{e}_{\min}$ as a function of the initial true anomaly ν_0 for a medium-high performance [Fig. 4(a)] and for a low performance [Fig. 4(b)] solar sail, assuming $T = 1\,\text{year}$ and a parking orbit coincident with the actual Earth's heliocentric orbit (i.e., $p_0 = 0.9997208\,\text{au}$ and $e_0 = 0.0167086$).

Circular parking orbit

In the special case when $e_0 = 0$, the coefficients c_1 and c_2 are independent of the parking orbit characteristics (i.e., the initial orbital radius r_0). In fact, Eqs. (13) yield

$$c_1 = \frac{\beta\,\left(2 + \lambda^2\right)}{2\,\left(1 + \lambda^2\right)} \quad , \quad c_2 = -\frac{\beta\,\lambda}{2\,\left(1 + \lambda^2\right)} \tag{25}$$

while Eqs. (23) reduce to

$$\widetilde{e}_{\max} = \frac{\beta}{2}\,\left(\sqrt{\frac{4 + \lambda^2}{1 + \lambda^2}} + 1\right) \quad , \quad \widetilde{e}_{\min} = \frac{\beta}{2}\,\left(\sqrt{\frac{4 + \lambda^2}{1 + \lambda^2}} - 1\right) \equiv \widetilde{e}_{\max} - \beta \tag{26}$$

that is, $\widetilde{e}_{\max}$ and $\widetilde{e}_{\min}$ are both proportional to the sail lightness number β. In particular, in the limiting case of time-invariant reflectivity, that is, when $T \to +\infty$ and $\{\epsilon,\, \lambda\} \to 0^+$, Eqs. (26) give $\widetilde{e}_{\max} \to 3\,\beta/2^-$ and $\widetilde{e}_{\min} \to \beta/2^+$. On the other hand, when the reflective film degrades immediately after the sail deployment, that is, when $T \to 0^+$ and $\{\epsilon,\, \lambda\} \to +\infty$, Eqs. (26)

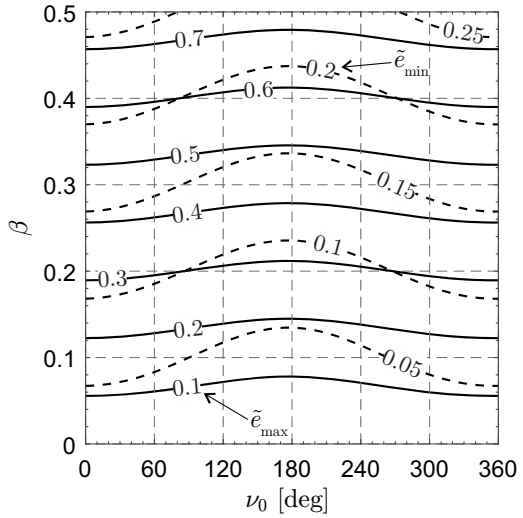

a) Medium-high performance solar sail.

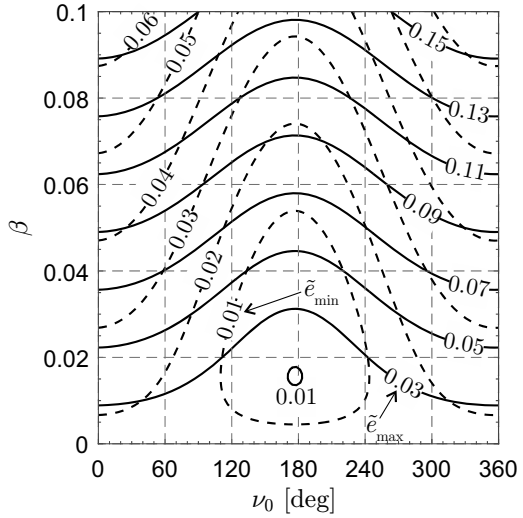

b) Low performance solar sail.

Figure 4 Variation of $\widetilde{e}_{\max}$ (solid line) and $\widetilde{e}_{\min}$ (dashed line) as a function of ν_0 when $p_0 = 0.9997208\,\text{au}$, $e_0 = 0.0167086$, and $T = 1\,\text{year}$.

give $\widetilde{e}_{\max} \to \beta^-$ and $\widetilde{e}_{\min} \to 0^+$. This behaviour is better illustrated in Fig. 5, which shows the variation of the ratios $\widetilde{e}_{\max}/\beta$ and $\widetilde{e}_{\min}/\beta$ with $\lambda \in [0, 5]$ for a circular parking orbit.

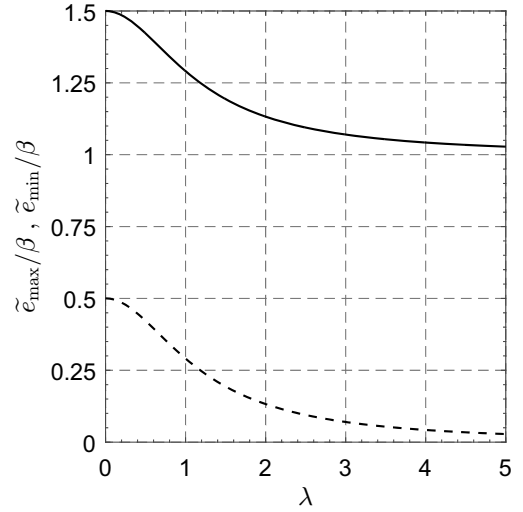

Figure 5 Variation of $\widetilde{e}_{\max}/\beta$ (solid line) and $\widetilde{e}_{\min}/\beta$ (dashed line) with λ when $e_0 = 0$.

The previous mathematical model is useful to obtain an estimation of the transfer performance in a heliocentric mission

case of a solar sail with a Sun-facing attitude, and considering the optical degradation of the reflective film. A possible mission application is discussed in the next section.

Mission applications

Consider a solar sail heliocentric transfer between a circular parking orbit of radius r_0 and a closed target orbit of given perihelion radius r_p (or aphelion radius r_a). In this case $p_0 \equiv r_0$ and, bearing in mind Eqs. (18), the expressions of r_p and r_a are

$$r_p = \frac{r_0}{1+\sqrt{\rho^2+(\rho')^2}} \quad , \quad r_a = \frac{r_0}{1-\sqrt{\rho^2+(\rho')^2}} \tag{27}$$

where ρ and ρ' are given by Eqs. (11) and (16), respectively, while $\{c_1,\, c_2\}$ are obtained from Eqs. (25). For a given value of T [or λ, see Eq. (10)], the ratio r_p/r_0 (or r_a/r_0) is a function of the pair $\{\theta,\, \beta\}$.

Figure 6 shows the variation of r_p/r_0 and r_a/r_0 as a function of $\beta \in [0,\, 1]$ and $\theta \in [0,\, 360]$ deg assuming a sail half-life $T = 1$ year (or $\lambda \simeq 0.1103$). The grey areas in the figure correspond to the pairs $\{\theta,\, \beta\}$ such that the spacecraft reaches an escape condition (i.e., $e \geq 1$). As expected, the minimum allowable value of r_p/r_0 is equal to 0.5.

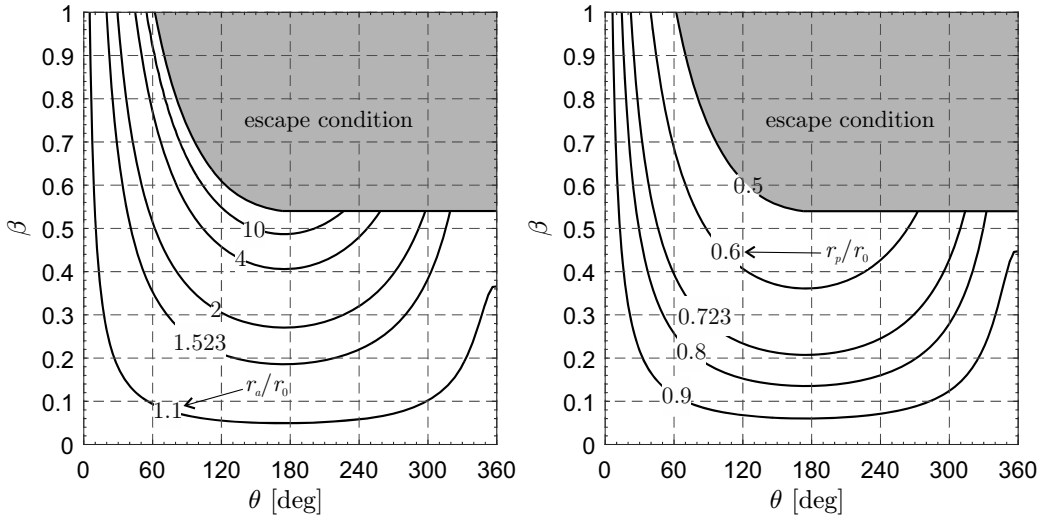

a) Dimensionless aphelion radius. **b)** Dimensionless perihelion radius.

Figure 6 Osculating orbit perihelion and aphelion radius for a circular parking orbit when $T = 1$ year.

For exemplary purposes, consider a transfer from a circular parking orbit with $r_0 = 1$ au to the orbit of Mars, which may be approximated to a circle with a radius of 1.523 au. The minimum value of the sail lightness number is approximately equal to 0.18 when the polar angle is slightly less than 180 deg; see Fig. 6(a). Likewise, in a simplified flyby mission to Venus (which is assumed to cover a circular orbit of radius 0.723 au), Fig. 6(b) gives a minimum value of β of about 0.2.

In both the previous cases, the sensitivity of the transfer performance to the sail film degradation half-life T (or λ) can be analyzed with the aid of Fig. 7. As expected, Fig. 7 shows that, for a given value of θ, the required lightness number decreases as T increases.

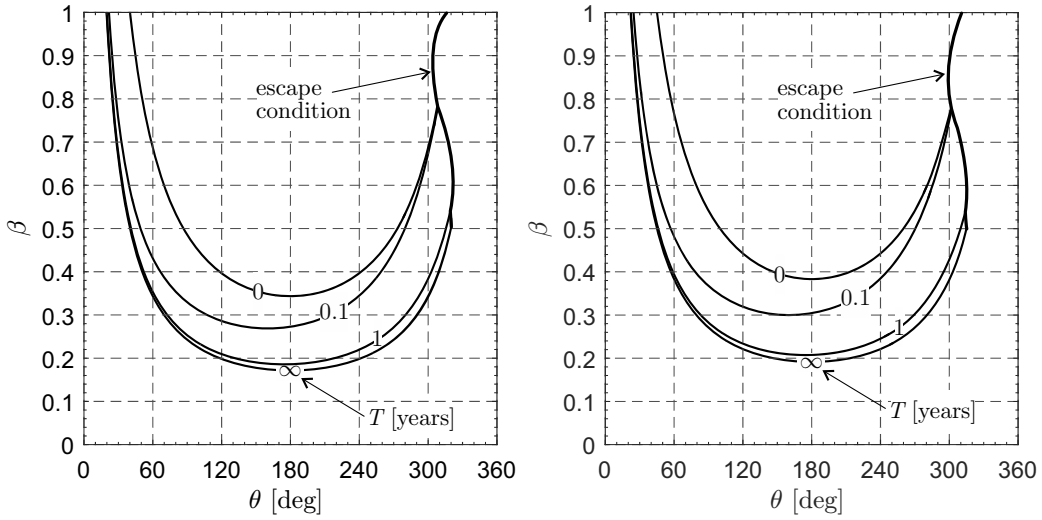

a) Mission to Mars. **b)** Mission to Venus.

Figure 7 Variation of β with θ and T in a flyby mission.

Conclusions

Closed-form solutions for the motion of a Sun-pointing solar sail with optical degradation have been discussed. In particular, the solar sail trajectory has been obtained in polar form, and the time variation of the orbital parameters has been derived as a function of the polar angle. In this context, the expression of the asymptotic (steady-state) spacecraft trajectory allows the maximum and minimum values of the osculating orbit eccentricity to be calculated in analytical form. In the simplified case of circular parking orbit, the solution is independent of the initial conditions and, in this case, the transfer performances in two typical interplanetary missions have been discussed with a graphical approach. It has been shown that the lightness number and the degradation half-life may be used as design parameters for a realistic solar sail-based mission scenario.

References

[1] Acord, J. D. and Nicklas, J. C., "Theoretical and practical aspects of solar pressure attitude control for interplanetary spacecraft," *Guidance and Control*, Vol. 13, Academic Press, 1964, pp. 73–101. doi: 10.1016/B978-0-12-395587-6.50008-9.

[2] Polyakhova, E. N., *Kosmicheskii polet s solnechnim parusom (Cosmic flight with solar sail)*, Nauka, Moscow, 1988.

[3] Wright, J. L., *Space Sailing*, Gordon and Breach Science, Philadelphia, 1992.

[4] McInnes, C. R., *Solar Sailing: Technology, Dynamics and Mission Applications*, Springer-Praxis Series in Space Science and Technology, Springer-Verlag, Berlin, 1999. doi: 10.1007/978-1-4471-3992-8.

[5] Fu, B., Sperber, E., and Eke, F., "Solar sail technology - A state of the art review," *Progress in Aerospace Sciences*, Vol. 86, October 2016, pp. 1–19. doi: 10.1016/j.paerosci.2016.07.001.

[6] Gong, S. and Macdonald, M., "Review on solar sail technology," *Astrodynamics*, Vol. 3, No. 2, June 2019, pp. 93–125. doi: 10.1007/s42064-019-0038-x.

[7] Vulpetti, G. and Scaglione, S., "Aurora project: estimation of the optical sail parameters," *Acta Astronautica*, Vol. 44, No. 2, January-February 1999, pp. 123–132. doi: 10.1016/S0094-5765(99)00038-7.

[8] Scaglione, S. and Vulpetti, G., "Aurora project: removal of plastic substrate to obtain an all-metal solar sail," *Acta Astronautica*, Vol. 44, No. 2, January-February 1999, pp. 147–150. doi: 10.1016/S0094-5765(99)00041-7.

[9] Khassanchine, R. H., Timofeev, A. N., Galygin, A. N., Kostiuk, V. I., and Tsvelev, V. M., "Influence of Electron Radiation on Outgassing of Spacecraft Materials," *Protection of Materials and Structures from the Space Environment*, edited by J. I. Kleiman, Springer Netherlands, Dordrecht, 2006, pp. 43–50. doi: 10.1007/1-4020-4319-8_5.

[10] Prosvirikov, V. M., Grigorevskiy, A. V., Kiseleva, L. V., Zelenkevich, A. P., and Tsvelev, V. M., "Influence of Space Environment on Spectral Optical Properties of Thermal Control Coatings," *Protection of Materials and Structures from the Space Environment*, edited by J. I. Kleiman, Springer Netherlands, Dordrecht, 2006, pp. 61–69. doi: 10.1007/1-4020-4319-8_7.

[11] Edwards, D. L., Semmel, C., Hovater, M., Nehls, M., Gray, P., Hubbs, W., and Wertz, G., "Status Of Solar Sail Material Characterization At Nasa's Marshall Space Flight Center," *Protection of Materials and Structures from the Space Environment*, edited by J. I. Kleiman, Springer Netherlands, Dordrecht, 2006, pp. 233–246. doi: 10.1007/1-4020-4319-8_22.

[12] Kezerashvili, R. Y. and Matloff, G. L., "Microscopic approach to analyze solar-sail space-environment effects," *Advances in Space Research*, Vol. 44, No. 7, October 2009, pp. 859–869. doi: 10.1016/j.asr.2009.05.002.

[13] Kezerashvili, R. Y., *Solar Sail: Materials and Space Environmental Effects*, Springer Berlin Heidelberg, Berlin, Heidelberg, 2014, pp. 573–592. doi: 10.1007/978-3-642-34907-2_36.

[14] Sznajder, M., Geppert, U., and Dudek, M. R., "Degradation of metallic surfaces under space conditions, with particular emphasis on Hydrogen recombination processes," *Advances in Space Research*, Vol. 56, No. 1, July 2015, pp. 71–84. doi: 10.1016/j.asr.2015.03.032.

[15] Sznajder, M., Geppert, U., and Marć, M., "Degradation of thin solar-sail membrane films under interplanetary medium," *Proceedings of The Fourth International Symposium on Solar Sailing*, Kyoto, Japan, January 17–20 2017.

[16] Sznajder, M., Geppert, U., and Dudek, M. R., "Hydrogen blistering under extreme radiation conditions," *npj Materials Degradation*, 2018. doi: 10.1038/s41529-017-0024-z.

[17] Ancona, E. and Kezerashvili, R. Y., "Temperature restrictions for materials used in aerospace industry for the near-Sun orbits," *Acta Astronautica*, Vol. 140, November 2017, pp. 565–569. doi: 10.1016/j.actaastro.2017.09.002.

[18] Pino, T., Circi, C., and Vulpetti, G., "Wrinkling analysis for small solar-photon sails: An experimental and analytic approach for trajectory design," *Advances in Space Research*, Vol. 63, No. 11, June 2019, pp. 3675–3690. doi: 10.1016/j.asr.2019.02.016.

[19] Rios-Reyes, L. and Scheeres, D. J., "Generalized model for solar sails," *Journal of Spacecraft and Rockets*, Vol. 42, No. 1, January-February 2005, pp. 182–185. doi: 10.2514/1.9054.

[20] Dachwald, B., Baturkin, V., Coverstone, V. L., Diedrich, B., Garbe, G. P., Görlich, M., Leipold, M., Luratt, F., Macdonald, M., McInnes, C. R., Mengali, G., Quarta, A. A., Rios-Reyes, L., Scheeres, D. J., Seboldt, W., and Wie, B., "Potential effects of optical solar sail degradation on trajectory design," *Proceedings of the AAS/AIAA Astrodynamics Conference*, South Lake Tahoe, CA, August 7–11 2005, AAS Paper 05-413.

[21] Dachwald, B., Seboldt, W., Macdonald, M., Mengali, G., Quarta, A. A., McInnes, C. R., Rios-Reyes, L., Scheere, D. J., Wie, B., Görlich, M., Lura, F., Diedrich, B., Baturkin, V., Coverstone, V. L., Leipold, M., and Garbe, G. P., "Potential solar sail degradation effects on trajectory and attitude control," *AIAA Guidance, Navigation, and Control Conference 2005*, San Francisco, CA, August 15–18 2005, Paper AIAA 2005-6172. doi: 10.2514/6.2005-6172.

[22] Dachwald, B., Mengali, G., Quarta, A. A., and Macdonald, M., "Parametric model and optimal control of solar sails with optical degradation," *Journal of Guidance, Control, and Dynamics*, Vol. 29, No. 5, September 2006, pp. 1170–1178. doi: 10.2514/1.20313.

[23] Dachwald, B., Macdonald, M., McInnes, C. R., Mengali, G., and Quarta, A. A., "Impact of optical degradation on solar sail mission performance," *Journal of Spacecraft and Rockets*, Vol. 44, No. 4, July 2007, pp. 740–749. doi: 10.2514/1.21432.

[24] McInnes, C. R., "Approximate closed-form solution for solar sail spiral trajectories with sail degradation," *Journal of Guidance, Control, and Dynamics*, Vol. 37, No. 6, November 2014, pp. 2053–2057. doi: 10.2514/1.G000225.

[25] McInnes, C. R., "Passive control of displaced solar sail orbits," *Journal of Guidance, Control, and Dynamics*, Vol. 21, No. 6, November-December 1998, pp. 975–982. doi: 10.2514/2.4334.

[26] Mengali, G. and Quarta, A. A., "Optimal heliostationary missions of high-performance sailcraft," *Acta Astronautica*, Vol. 60, No. 8-9, April-May 2007, pp. 676–683. doi: 10.1016/j.actaastro.2006.07.018.

[27] McInnes, C. R., "Artificial Lagrange points for a partially reflecting flat solar sail," *Journal of Guidance, Control, and Dynamics*, Vol. 22, No. 1, January-February 1999, pp. 185–187. doi: 10.2514/2.7627.

[28] Aliasi, G., Mengali, G., and Quarta, A. A., "Passive control feasibility of collinear equilibrium points with solar balloons," *Journal of Guidance, Control, and Dynamics*, Vol. 35, No. 5, September-October 2012, pp. 1657–1661. doi: 10.2514/1.57393.

[29] Aliasi, G., Mengali, G., and Quarta, A. A., "Artificial Lagrange points for solar sail with electrochromic material panels," *Journal of Guidance, Control, and Dynamics*, Vol. 36, No. 5, September-October 2013, pp. 1544–1550. doi: 10.2514/1.58167.

[30] Mengali, G., Quarta, A. A., and Denti, E., "Optimal in-orbit repositioning of Sun-pointing Smart Dust," *Acta Astronautica*, Vol. 154, January 2019, pp. 278–285. doi: 10.1016/j.actaastro.2018.03.036.

[31] McInnes, C. R., *Solar Sailing: Technology, Dynamics and Mission Applications*, Springer-Praxis Series in Space Science and Technology, Springer-Verlag, Berlin, 1999, pp. 38–40. doi: 10.1007/978-1-4471-3992-8.

[32] Bürdet, C. A., "Le mouvement Keplerien et les oscillateurs harmoniques," *Journal für die reine und angewandte Mathematik*, Vol. 1969, No. 238, January 1969, pp. 71–84. doi: 10.1515/crll.1969.238.71.

[33] Ferrándiz, J. M., "A general canonical transformation increasing the number of variables with application to the two-body problem," *Celestial Mechanics and Dynamical Astronomy*, Vol. 41, No. 1–4, March 1987, pp. 343–357. doi: 10.1007/BF01238770.

[34] Ferrándiz, J. M., Sansaturio, M. E., and Pojman, J. R., "Increased accuracy of computations in the main satellite problem through linearization methods," *Celestial Mechanics and Dynamical Astronomy*, Vol. 53, No. 4, December 1992, pp. 347–363. doi: 10.1007/BF00051816.

[35] Fukushima, T., "New Two-Body Regularization," *The Astronomical Journal*, Vol. 133, No. 1, January 2007, pp. 1–10. doi: 10.1086/509606.